Title: Visualizing reactive astrogliosis extends survival in glioblastoma patients

Authors: Hae Young Ko[1,2]†, Jee-In Chung[1]†, Dongwoo Kim[1]†, Yongmin Mason Park[3,4], Han Hee Jo[1], Sangwon Lee[1], Seon Yoo Kim[1], Jisu Kim[1], Joong-Hyun Chun[1], Kyung-Seok Han[5], Misu Lee[6], Yeonha Ju[3,4], Sun Jun Park[7,8], Ki Duk Park[7,8], Min-Ho Nam[9,10], Se Hoon Kim[11], Jong Hee Chang[12]*, C. Justin Lee[3,4]*, Mijin Yun[1]*

[1]Department of Nuclear Medicine, Severance Hospital, Yonsei University College of Medicine, Seoul 03722, Republic of Korea.

[2]CONNECT-AI Research Center, Yonsei University College of Medicine, Seoul 03722, Republic of Korea.

[3]Center for Cognition and Sociality, Institute for Basic Science, Daejeon 34126, Republic of Korea.

[4]IBS School, University of Science and Technology, Daejeon 34126, Republic of Korea

[5]Department of Medical Biotechnology, Dongguk University-Gyeongju, Gyeongju 38066, Republic of Korea.

[6]Division of Life Science, College of Life Science and Bioengineering, Incheon National University, Incheon 22012, Republic of Korea.

[7]Convergence Research Center for Diagnosis, Treatment and Care System of Dementia, Korea Institute of Science and Technology (KIST), Seoul 02792, Republic of Korea.

[8]Division of Bio-Med Science & Technology, KIST School, Korea University of Science and Technology, Seoul 02792, Republic of Korea.

[9]Center for Neuroscience, KIST, Seoul 02792, Republic of Korea.

[10]Department of KHU-KIST Convergence Science and Technology, Kyung Hee University, Seoul 02447, Republic of Korea.

[11]Department of Pathology, Severance Hospital, Yonsei University College of Medicine, Seoul 03722, South Korea

[12]Department of Neurosurgery, Severance Hospital, Yonsei University College of Medicine, Seoul 03722, Republic of Korea.

*Correspondence to: Jong Hee Chang (changjh@yuhs.ac), C. Justin Lee (cjl@ibs.re.kr), or Mijin Yun (yunmijin@yuhs.ac),

† These authors equally contributed to this study.

ABSTRACT

Glioblastoma is a devastating brain tumor with dismal prognosis of only 15-month survival regardless of surgical resection with few alternatives. Here, we report a reactive astrogliosis-targeted neuroimaging technique using the fusion of ^{11}C-acetate PET and MRI (AcePET) extended the overall survival of patients by 5.25 months compared to conventional MRI-guided surgery. Targeted biopsy of ^{11}C-acetate uptake-increased regions showed the signs of reactive astrogliosis with cancer stem cells at the boundary of high-grade gliomas. The appearance of marginal reactive astrogliosis and MCT1-dependent ^{11}C-acetate uptake was recapitulated in U87MG-orthotophic models. U87MG-derived excessive glutamate caused reactive astrogliosis and aberrant astrocytic GABA-release, which subsequently reduced neuronal glucose uptake through glucose transporter-3 (GLUT3). We propose AcePET-guided surgery, visualizing reactive astrogliosis, as an advanced surgical strategy to improve glioblastoma patient survival.

One-Sentence Summary: AcePET-guided surgery extends patient survival by visualizing reactive astrogliosis at the tumor margin

Main Text

Glioblastoma multiforme, the most aggressive type of glioma with a median overall survival (OS) of about 15 months, accounts for the majority of primary malignant tumors in the brain (*1*). Currently, surgical resection is the standard treatment modality, accompanied with determination of resection margin based on magnetic resonance imaging (MRI). The strongest evidence for the use of T1 gadolinium-enhanced MRI comes from a randomized controlled trial: A complete resection of contrast-enhanced tumor resulted in longer OS compared to an incomplete resection (*2*). However, regardless of the complete surgical resection based on MRI, recurrence happens in almost all cases mostly at the margin of resection cavity in the peri-tumoral area (*3*). Therefore, methods that easily and clearly detect the tumor margin during surgery would be extremely beneficial to prevent recurrence.

As the latest technology, 5-aminolevulinic acid (5-ALA) fluorescence-guided surgery has been helpful for surgeons to identify the apparent tumor margin intraoperatively (*4*). A meta-analysis yielded a pooled OS difference of 3.05 months, favouring 5-ALA-guided surgery compared with control groups without 5-ALA (*5*). However, one of the major limitations of 5-ALA-guided surgery is the low tumor-cell density in the infiltrating margin, causing an insufficient 5-ALA uptake and vague boundary fluorescence (*6*). To make matters worse, false-positive fluorescence is common due to the leakage of fluorescent molecules into the extracellular matrix (*7*). Despite the assistance of 5-ALA fluorescence, a complete resection of infiltrating, scattered cancer cells in the peri-tumoral region beyond fluorescence margin is still difficult to achieve. Therefore, there is a desperate need for advanced imaging techniques to clearly visualize the peri-tumoral infiltrating cancer cells for more complete resection and to extend patient survival.

In addition to cancer stem cells, there are many non-tumorous cells such as microglia/macrophages, astrocytes, neutrophils, dendritic cells, endothelial cells in the tumor microenvironment (TME) (*8*). In particular, reactive astrocytes, one of the major cell types in TME, are located around the tumor boundary and thought to enhance the proliferation and invasion of glioblastomas by secreting cytokines and chemokines (*9-12*). Thus, it would be highly advantageous to develop a functional imaging technique to visualize reactive astrogliosis *in vivo* and aid image-guided surgery for complete tumor resection. However, there has been no clinically available molecular probe to specifically image reactive astrocytes surrounding the glioblastoma. Astrocytes are known to utilize acetate as a metabolic substrate and transport it

mainly through the monocarboxylate transporter-1 (MCT1) (*13-15*). ^{11}C–acetate, a radiotracer version of acetate, is already in clinical use or under clinical trial for detecting the acetate-dependent low-grade, but not high-grade, tumor cells of hepatocellular carcinoma, renal cell carcinoma, and prostate cancer (*16*). Unexpectedly, we have previously discovered a high ^{11}C-acetate uptake in high-grade gliomas, but not low-grade gliomas (*17*). However, the high-grade glioma cells do not appear to take up ^{11}C-acetate directly (*17*), raising a possibility that cells other than tumor cells such as reactive astrocytes might take up ^{11}C-acetate on positron emission tomography/computed tomography (PET/CT). In this study, we investigated whether the reactive astrocytes surrounding the gliomas take up high levels of ^{11}C-acetate, and assessed the OS of patients with high-grade gliomas who underwent AcePET-guided surgery.

To compare the OS of glioma patients, we performed a Kaplan-Meier survival curve analysis on patients who underwent conventional MRI-guided surgery versus AcePET-guided surgery. In detail, AcePET-guided surgery was performed as the neurosurgeon was navigated by the fusion images of ^{11}C-acetate PET and MRI. There were 149 glioma patients with at least 2-year follow-up after surgery and received appropriate treatment according to the grade of tumor (fig. S1A, table S1). The patients were divided into three groups depending on the grade of tumor and the presence of the mutation (p.R132H) in isocitrate dehydrogenase 1 gene (IDH1-mt), which has been shown to exhibit a favorable disease outcome compared with its wild-type counterpart (IDH1-WT) (*18*); 1) Grade II gliomas (N=41), 2) IDH1-mt high-grade gliomas (N=28), and 3) IDH1-WT high-grade gliomas (N=80)(Fig. 1A). The patients with low-grade and IDH1-mt gliomas did not show any fatality and were not included in the survival analysis (fig. S1A). In the IDH1-WT high-grade glioma group, 37 patients received AcePET-guided surgery and remaining 43 patients, MRI-guided surgery. After propensity score matching (table S3), we found a significantly prolonged OS in patients with AcePET-guided surgery than MRI-guided surgery. The AcePET-guided surgery extended the median OS by 5.25 months from 16.75 to 22.00 months and 2-year survival rate by 12.5% from 29.2% to 41.7% (Fig. 1A). Moreover, the progression-free survival (PFS) was extended by 10.68 months from 8.25 to 18.93 months (fig. S1B), suggesting a better local tumor removal by AcePET-guided surgery. These results raise a possibility that AcePET-guided surgery provides more accurate tumor boundary and more complete resection than conventional MRI-guided surgery in IDH1-WT high-grade glioma patients.

To test this possibility, we compared tumor volumes between ^{11}C-acetate PET and MRI images in IDH1-WT high-grade gliomas. On visual inspection, IDH1-WT high-grade gliomas showed significantly higher ^{11}C-acetate uptake at the periphery of the tumor (Fig. 1B, red demarcation; Fig. 1C), while low-grade or IDH1-mt tumors demonstrated no remarkable or minimal ^{11}C-acetate uptake. The calculated tumor volume by ^{11}C-acetate PET was significantly larger than that by contrast-enhanced MRI (Fig. 1B, blue demarcation) in IDH1-WT high-grade gliomas (Fig. 1D). These results indicate that ^{11}C-acetate PET exhibits a clear and larger tumor boundary beyond the contrast-enhanced MRI, providing a plausible explanation for the extended OS and PFS by AcePET-guided surgery.

To investigate whether reactive astrogliosis is present at the high ^{11}C-acetate uptake-regions, we performed double-immunohistochemistry with the targeted biopsy tissues of high- and low-grade gliomas using antibodies against glial fibrillary acidic protein (GFAP), an astrocyte marker, and Ki-67, a marker for proliferating cells (Fig. 1E, F). In IDH1-WT high-grade glioma, we distinguished three distinct regions depending on the presence of tumor and GFAP-positive astrocytic morphology; (T) tumor region with amoeboid-shaped astrocytes, (L) region with line-shaped astrocytes, and (S) region with star-shaped astrocytes (Fig. 1, E and G, fig. S2A). The tangential line-shaped astrocytes (fig. S2B) delineated the boundary between T and S regions to form a glial scar-like barrier around the tumor. In contrast, we found only S region with star-shaped astrocytes, but not L region, in low-grade or IDH1-mt gliomas (Fig. 1, F and H). The reactivity of astrocytes at the margin of gliomas was more severe in high-grade gliomas than in low-grade or IDH1-mt gliomas, as evidenced by higher expressions of both GFAP and MAO-B, a recently identified reactive astrocyte marker (*19*) (Fig. 1, G, J and L). MCT1, a potential transporter of acetate in astrocytes (*15, 20*), was found to be expressed at high level in the periphery of IDH1-WT high-grade gliomas, but almost absent in low-grade or IDH1-mt gliomas (Fig. 1, G, H and M), which was consistent with the ^{11}C-acetate uptake results (Fig. 1, B and C). We found numerous Ki-67-positive cells in the L and S regions of high-grade gliomas (Fig. 1, E, G and K) but not in low-grade or IDH1-mt gliomas (Fig. 1, F, H and K). The Ki-67-positive cells were mostly co-localized with CD133, the marker for cancer stem cell (*21*) (Fig. 1, I and N), indicating the existence of cancer stem cells within the region of reactive astrocytes at the tumor margin. Taken together, these results suggest that the extended OS and PFS in the patients who underwent AcePET-guided surgery are likely due to more efficient removal of the cancer stem cells within the regions of reactive astrogliosis.

To delineate the molecular and cellular mechanism of elevated ^{11}C-acetate uptake in peri-tumoral region of high-grade glioma, we employed a reverse-translational approach and performed ^{11}C-acetate microPET imaging and ^{14}C-acetate autoradiography in orthotopic mouse tumor models. We used two types of human glioma cell lines; U87MG cell line to mimic high-grade glioma and U87-IDH1-mt (U87mt) to mimic IDH1-mt glioma. We placed a region-of-interest (ROI) over the peri-tumoral and mirror-image contralateral regions to measure the standard uptake value (SUV) ratio on ^{11}C-acetate microPET images. We found a significantly higher SUV ratio in the peri-tumoral region in U87MG model compared to U87mt model (Fig. 2, A and E). We then asked whether the elevated ^{11}C-acetate uptake is associated with reactive astrogliosis and astrocytic MCT1 level. To assess the reactive astrogliosis in U87MG and U87mt models, we immunostained with antibodies against GFAP, S100β (another reactive astrocyte marker), MAO-B, and MCT1(Fig. 2, B to D). Similar to human gliomas, U87MG model showed significantly higher intensity and a larger area of GFAP and S100β immunoreactivities than those of U87mt model (Fig. 2, F and G). MAO-B and MCT1 levels in GFAP- and S100β-positive areas in the peri-tumoral region were significantly higher in U87MG than in U87mt models (Fig. 2, C, D, I and J). These results indicate that ^{11}C-acetate uptake was positively correlated with both reactive astrogliosis and astrocytic MCT1.

To test whether reactive astrogliosis is necessary for the elevated ^{11}C-acetate uptake in U87MG model, we used a selective and reversible MAO-B inhibitor KDS2010, which has been shown to block reactive astrogliosis in animal models of Alzheimer's disease, Parkinson's disease, and subcortical stoke in our previous reports (*19, 22-24*). After oral administration of KDS2010, we found a significantly decreased ^{11}C-acetate uptake on microPET images and ^{14}C-acetate uptake on autoradiography at the peri-tumoral regions (Fig. 2, K and L). In addition, GFAP, S100β, MAO-B, and MCT1 levels in reactive astrocytes were all significantly reduced after KDS2010 treatment (Fig. 2, M to Q and fig. S3, A to C). These results indicate that reactive astrogliosis is necessary for the elevated ^{11}C-acetate uptake.

To test whether astrocytic MCT1 is necessary for the ^{11}C-acetate uptake, we adopted a cre-loxp-dependent, astrocyte-specific gene-silencing of MCT1 using AAV-GFAP-cre-mCherry and AAV-pSico-rMCT1sh-GFP viruses around the tumor in U87MG model. We found that gene-silencing of MCT1 significantly decreased ^{11}C-acetate uptake on microPET images and ^{14}C-acetate uptake on autoradiography at the peri-tumoral regions (Fig. 2, R and S). In addition, the levels of GFAP, S100β, and MAO-B were significantly reduced by the astrocytic gene-silencing of MCT1 (Fig. 2, T to X and fig. S3, D to F), indicating that

astrocytic MCT1 is necessary for the elevated ^{11}C-acetate uptake. Taken together, the elevated ^{11}C-acetate uptake requires reactive astrogliosis and astrocytic MCT1 at the boundary of high-grade tumor.

To delineate the detailed molecular and cellular mechanisms of the elevated acetate uptake, we performed various *in vitro* biochemical and physiological assays with U87MG and mouse primary astrocytes (AST). We first screened for the cell types that show a high level of MCT1. We found that AST showed much higher expression of MCT1 along with GFAP and MAO-B than various glioma cell lines, including U87MG, U373MG, T98G, and U87mt (Fig. 3A). Consistently, AST showed much higher ^{14}C-acetate uptake compared to those glioma cell lines (Fig. 3B). These results implicate that the cellular origin of the enhanced acetate uptake is most likely astrocytes rather than tumor cells. To identify the tumor-derived molecular factors that induce reactive astrogliosis, we obtained conditioned media (CM) from U87MG or U87mt cells and applied to AST (fig. S4A). U87MG-CM, but not U87mt-CM, significantly augmented the protein or mRNA of MAO-B and MCT1 expression (Fig. 3, C and D) and ^{14}C-acetate uptake (Fig. 3E). Gene-silencing of MCT1 in AST (fig. S4B) significantly prevented the augmented ^{14}C-acetate uptake induced by U87MG-CM (Fig. 3F), indicating that MCT1 mediates the acetate uptake.

To test if glutamate could be one of the tumor-derived molecular factors, we directly measured the amount of glutamate in U87MG-CM and U87mt-CM using a glutamate assay kit. We found a significantly higher level of glutamate in U87MG-CM than U87mt-CM (Fig. 3G), consistent with a previous report showing that U87MG cells secrete excessive amount of glutamate (*25*). To test if individual tumor cells release glutamate in Ca^{2+}-dependent manner, we measured Ca^{2+} signals using Fura-2AM and glutamate release using iGluSnFR (*26*), a fluorescent glutamate biosensor, upon PAR1 activation by TFLLR-pressure-application as previously described (*27*) (fig. S4C). We found that TFLLR elicited a significantly higher glutamate release from individual U87MG than U87mt cells (Fig. 3, H and I), without affecting the Ca^{2+} responses (Fig. 3, J and K). To investigate whether glutamate alone can induce reactive astrogliosis and elevated acetate uptake, we treated astrocytes with varying concentrations of glutamate. We found increased protein levels of GFAP, MAO-B, and MCT1 (Fig. 3L) and increased ^{14}C-acetate uptake in concentration-dependent manner (Fig. 3M and fig. S4D). To determine which type of glutamate receptor in astrocyte is responsible for reactive astrogliosis and acetate uptake, we treated astrocytes with U87MG-CM in the presence of APV, CNQX, or MPEP inhibitors of NMDA, AMPA, and mGluR5 receptors,

respectively (Fig. 3N). We found that the U87MG-CM-induced increase in MCT1, but not MAO-B, was reduced by APV, CNQX, and MPEP (Fig. 3N). These results indicate that the tumor-derived glutamate causes elevated acetate uptake, but not reactive astrogliosis, through activation of glutamate receptors. Consistently, U87MG-CM-induced increase in ^{14}C-acetate uptake was significantly blocked by the inhibitors of glutamate receptors (Fig. 3O and fig. S4E). Altogether, these results indicate that glutamate is the major factor derived from high-grade glioma cells to induce reactive astrogliosis and elevated acetate uptake.

How does glutamate cause reactive astrogliosis? We have shown that tumor-derived glutamate causes an increase in MAO-B, independently of glutamate receptors. This raises an interesting possibility that excessive glutamate after taken up by astrocytes, can cause MAO-B-dependent GABA-synthesis and -release, which are closely associated with reactive astrogliosis (*19, 28, 29*). To test this possibility, we performed sniffer-patch with GABAc-expressing HEK293T cell as a biosensor for GABA as previously described (Fig. 3P) (*30*). We found that poking-induced, Ca^{2+}-dependent GABA-release was significantly enhanced after 2-day incubation with 10 mM glutamate compared with control (Fig. 3, Q and R). These findings lead us to postulate a mechanistic model in which the high-grade glioma-derived excessive glutamate 1) activates glutamate receptors to increase MCT1-expression and acetate uptake, and 2) results in glutamate uptake, possibly via glutamate transporter (EAAT), and 3) causes reactive astrogliosis via MAO-B dependent GABA-synthesis and GABA-release, possibly via Best1, in astrocytes (Fig. 3S).

What is the role of GABA from reactive astrocytes? We have previously shown that GABA from reactive astrocytes causes cortical glucose hypometabolism and impedes functional recovery after subcortical stroke (*22*). In addition, we have recently demonstrated the reactive astrogliosis-mediated glucose hypometabolism via reduction in neuronal glucose transporter GLUT3 in Alzheimer's disease patients (*31*). To test if the similar mechanisms exist in high-grade glioma, we measured the level of GLUT3 in *in vitro* neuron-glia co-culture, *in vivo* animal model, and glioma patients. In *in vitro* co-culture system, we found that U87MG-CM treatment caused a significant decrease in the protein levels of neuronal nuclear protein (NeuN) and GLUT3 in a time-dependent manner, along with an increase in GFAP, MAO-B, and MCT1 (Fig. 4A). In U87MG and U87mt models, we found a significantly higher level of astrocytic GABA (Fig. 4, B and D) and lower level of neuronal GLUT3 (Fig. 4, C and E) in the peri-tumoral regions of U87MG model compared to U87mt model. In glioma patients, we found a remarkable decrease in ^{18}F-fluorodeoxyglucose (FDG) uptake on PET/CT

images at the adjacent cortical regions beyond the tumor boundary, delineated by ^{11}C-acetate PET/CT in IDH1-WT high-grade glioma patients, but not in IDH1-mt or low-grade glioma patients (Fig. 4F). In the targeted biopsy tissues, we found a significantly lower level of neuronal GLUT3 in IDH1-WT high-grade glioma than that of IDH1-mt or low-grade glioma (Fig. 4, G and I). In marked contrast, we observed a high level of GLUT1 in high-grade glioma, but not in IDH1-mt or low-grade glioma (Fig. 4, H and J). These results indicate that the aberrant GABA from reactive astrocytes induces neuronal glucose hypometabolism. Taken together, these findings lead us to further postulate a multicellular mechanistic model, consisting of high-grade glioma cells to gorge on glucose and release excessive glutamate, reactive astrocytes to release aberrant GABA, and neighbouring neurons with suppressed glucose metabolism (Fig. 4K).

One of the most striking findings in our study is that AcePET-guided surgery significantly extended survival in patients with high-grade glioma by 5.25 months of OS and 10.68 months of PSF. This astonishing improvement in patient survival is most likely due to more complete removal of cancer stem cells within the regions of reactive astrogliosis beyond the tumor boundary on MRI. Cancer stem cells at the leading edge of tumor play critical roles in rapid expansion and invasion into adjacent normal brain tissue (*32*). After surgery, the left-over cancer stem cells are known to be responsible for tumor recurrence (*33*). Our AcePET-guided surgery provides significant advantages over the conventional MRI- or fluorescence-guided surgery, which is constrained by the lack of visualization of reactive astrogliosis and infiltrating cancer stem cells at the leading edges of tumor (*34*).

In this study, we have identified the abnormal multicellular interactions through communicating molecules between high-grade glioma cells and reactive astrocytes via excessive glutamate, and between reactive astrocytes and neighbouring neurons via aberrant GABA in TME. The source of such abnormal molecular and cellular communications is possibly originated from the monopoly of glucose uptake by high-grade gliomas for aggressive tumor proliferation (Fig. 4E, ^{18}F-FDG PET). Because of the devouring of glucose by high-grade gliomas, the surrounding astrocytes are devoid of available glucose and forced to utilize alternative metabolites such as acetate. Unfortunately, the increased acetate and glutamate uptake in reactive astrocytes lead to aberrant production and release of GABA onto neighbouring neurons which are strongly suppressed by GABA and become metabolically poor without glucose. The neuronal hypometabolism and increased inhibitory tone inadvertently result in neuronal dysfunction and cognitive impairment that are often observed in glioma patients. We

have identified several molecular targets which can be therapeutically beneficial. For example, inhibiting GABA production via MAO-B in reactive astrocytes should improve the neuronal dysfunction and cognitive impairment. As in IDH1-mt glioma, preventing glutamate production and release from high-grade glioma cells should ameliorate the toxic environment in TME. Finally, preventing the monopoly of glucose by high-grade glioma cells via GLUT1 should stop the cascade of events that leads to reactive astrogliosis and neuronal hypometabolism. These exciting possibilities await future investigations.

Acknowledgments: The schematic figure (Fig. 3S and 4K) was drawn using Biorender.

Funding: This study was supported by IBS-R001-D2 from the Institute for Basic Science funded by the Korean Ministry of Science and ICT to C.J.L.; NRF-2018M3C7A1056898 and NRF-2020R1A2B5B01098109 from National Research Foundation (NRF) of Korea to M.Y.; NRF-2021R1C1C2011016 to H.Y.K.

Author contributions: C.J.L. and M.Y. designed the study. D.K., J.H.C. and M.Y. conceived the idea of AcePET-guided surgery. H.Y.K., D.K., J.C., C.J.L. and M.Y. wrote the manuscript. J.H.C. performed surgeries. D.K managed patient samples and performed statistical analysis in patients. H.Y.K. acquired and analyzed animal images. J.C., H.H.J., S.Y.K., J.K. and M.L. performed and analyzed histological staining. J.C. and H.H.J. performed and analyzed western blot and quantitative RT-PCR. Y.M.P and K.H. performed glutamate and calcium imaging. Y.M.P and Y.J performed sniffer patch. Y.M.P and M.H.N. prepared viruses. S.L analyzed PET and MRI images. J.H.C. provided ^{11}C-acetate. S.J.P. and K.E.P. provided KDS2010. S.H.K. performed pathological studies in patient tissues. All authors contributed to writing and provided feedback.

Competing interests: The authors declare that they have no conflict of interest.

Data and materials availability: All data is available in the main text or the supplementary materials upon any reasonable requests.

Supplementary Materials:

Materials and Methods

Figures S1-S4

Tables S1-S5

References (*1-6*)

References and notes

1. E. G. Van Meir *et al.*, Exciting new advances in neuro-oncology: the avenue to a cure for malignant glioma. *CA Cancer J Clin* **60**, 166-193 (2010).
2. U. Pichlmeier, A. Bink, G. Schackert, W. Stummer, A. L. A. G. S. Group, Resection and survival in glioblastoma multiforme: an RTOG recursive partitioning analysis of ALA study patients. *Neuro Oncol* **10**, 1025-1034 (2008).
3. K. Petrecca, M. C. Guiot, V. Panet-Raymond, L. Souhami, Failure pattern following complete resection plus radiotherapy and temozolomide is at the resection margin in patients with glioblastoma. *J Neurooncol* **111**, 19-23 (2013).
4. W. Stummer *et al.*, Fluorescence-guided resection of glioblastoma multiforme by using 5-aminolevulinic acid-induced porphyrins: a prospective study in 52 consecutive patients. *J Neurosurg* **93**, 1003-1013 (2000).
5. S. Gandhi *et al.*, Survival Outcomes Among Patients With High-Grade Glioma Treated With 5-Aminolevulinic Acid-Guided Surgery: A Systematic Review and Meta-Analysis. *Front Oncol* **9**, (2019).
6. S. Utsuki *et al.*, Possibility of using laser spectroscopy for the intraoperative detection of nonfluorescing brain tumors and the boundaries of brain tumor infiltrates - Technical note. *Journal of Neurosurgery* **104**, 618-620 (2006).
7. S. Utsuki *et al.*, Histological examination of false positive tissue resection using 5-aminolevulinic acid-induced fluorescence guidance. *Neurol Med-Chir* **47**, 210-213 (2007).
8. D. F. Quail, J. A. Joyce, The Microenvironmental Landscape of Brain Tumors. *Cancer Cell* **31**, 326-341 (2017).
9. G. Nagashima, R. Suzuki, J. Asai, T. Fujimoto, Immunohistochemical analysis of reactive astrocytes around glioblastoma: an immunohistochemical study of postmortem glioblastoma cases. *Clin Neurol Neurosurg* **104**, 125-131 (2002).
10. J. Lee, A. K. Borboa, A. Baird, B. P. Eliceiri, Non-invasive quantification of brain tumor-induced astrogliosis. *BMC Neurosci* **12**, 9 (2011).
11. A. L. Placone, A. Quinones-Hinojosa, P. C. Searson, The role of astrocytes in the progression of brain cancer: complicating the picture of the tumor microenvironment. *Tumour Biol* **37**, 61-69 (2016).
12. D. M. Le *et al.*, Exploitation of astrocytes by glioma cells to facilitate invasiveness: a mechanism involving matrix metalloproteinase-2 and the urokinase-type plasminogen activator-plasmin cascade. *J Neurosci* **23**, 4034-4043 (2003).
13. S. Cerdan, B. Kunnecke, J. Seelig, Cerebral metabolism of [1,2-13C2]acetate as detected by in vivo and in vitro 13C NMR. *J Biol Chem* **265**, 12916-12926 (1990).
14. B. Hassel, U. Sonnewald, F. Fonnum, Glial-neuronal interactions as studied by cerebral metabolism of [2-13C]acetate and [1-13C]glucose: an ex vivo 13C NMR spectroscopic study. *J Neurochem* **64**, 2773-2782 (1995).
15. R. A. Waniewski, D. L. Martin, Preferential utilization of acetate by astrocytes is attributable to transport. *J Neurosci* **18**, 5225-5233 (1998).
16. M. Yun *et al.*, The importance of acetyl coenzyme A synthetase for 11C-acetate uptake and cell survival in hepatocellular carcinoma. *J Nucl Med* **50**, 1222-1228 (2009).
17. S. Kim *et al.*, The roles of (11)C-acetate PET/CT in predicting tumor differentiation and survival in patients with cerebral glioma. *European journal of nuclear medicine and molecular imaging* **45**, 1012-1020 (2018).
18. D. N. Louis *et al.*, The 2016 World Health Organization Classification of Tumors of the Central Nervous System: a summary. *Acta Neuropathol* **131**, 803-820 (2016).
19. S. Jo *et al.*, GABA from reactive astrocytes impairs memory in mouse models of Alzheimer's disease. *Nat Med* **20**, 886-896 (2014).

20. J. Y. Jeon *et al.*, Regulation of Acetate Utilization by Monocarboxylate Transporter 1 (MCT1) in Hepatocellular Carcinoma (HCC). *Oncol Res* **26**, 71-81 (2018).
21. G. Liu *et al.*, Analysis of gene expression and chemoresistance of CD133+ cancer stem cells in glioblastoma. *Mol Cancer* **5**, 67 (2006).
22. M. H. Nam *et al.*, Excessive Astrocytic GABA Causes Cortical Hypometabolism and Impedes Functional Recovery after Subcortical Stroke (vol 32, pg 107861, 2020). *Cell Rep* **32**, (2020).
23. J. H. Park *et al.*, Newly developed reversible MAO-B inhibitor circumvents the shortcomings of irreversible inhibitors in Alzheimer's disease. *Sci Adv* **5**, eaav0316 (2019).
24. J. Y. Heo *et al.*, Aberrant Tonic Inhibition of Dopaminergic Neuronal Activity Causes Motor Symptoms in Animal Models of Parkinson's Disease. *Curr Biol* **30**, 276-291 e279 (2020).
25. Z. C. Ye, H. Sontheimer, Glioma cells release excitotoxic concentrations of glutamate. *Cancer Res* **59**, 4383-4391 (1999).
26. J. S. Marvin *et al.*, An optimized fluorescent probe for visualizing glutamate neurotransmission. *Nat Methods* **10**, 162-170 (2013).
27. D. H. Woo *et al.*, TREK-1 and Best1 channels mediate fast and slow glutamate release in astrocytes upon GPCR activation. *Cell* **151**, 25-40 (2012).
28. H. Chun *et al.*, Severe reactive astrocytes precipitate pathological hallmarks of Alzheimer's disease via H2O2(-) production. *Nat Neurosci* **23**, 1555-1566 (2020).
29. H. Chun, C. J. Lee, Reactive astrocytes in Alzheimer's disease: A double-edged sword. *Neurosci Res* **126**, 44-52 (2018).
30. S. J. Oh *et al.*, Ultrasonic Neuromodulation via Astrocytic TRPA1. *Curr Biol* **29**, 3386-3401 e3388 (2019).
31. M. H. Nam, et al., PET/CT imaging reveals reactive astrocyte-mediated neuronal hypometabolism in Alzheimer's disease patients. *Nat Med*, (under review).
32. A. K. Croker, A. L. Allan, Cancer stem cells: implications for the progression and treatment of metastatic disease. *J Cell Mol Med* **12**, 374-390 (2008).
33. E. Batlle, H. Clevers, Cancer stem cells revisited. *Nat Med* **23**, 1124-1134 (2017).
34. M. Ji *et al.*, Detection of human brain tumor infiltration with quantitative stimulated Raman scattering microscopy. *Sci Transl Med* **7**, 309ra163 (2015).

Figures

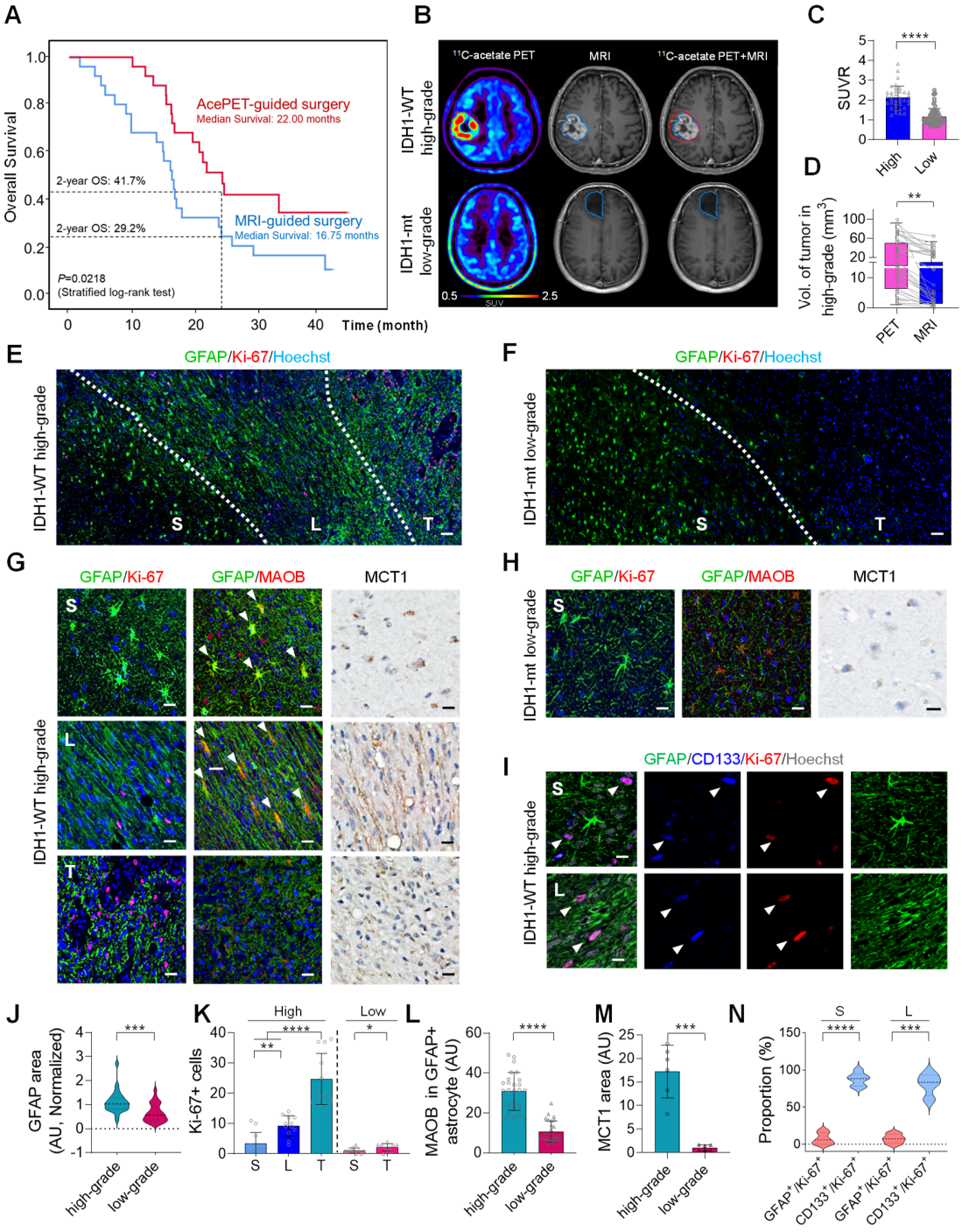

Figure 1. AcePET-guided surgery extends overall survival and reveals reactive astrogliosis at the tumor boundary in high-grade glioma patients. (**A**) AcePET-guided surgery extended the median OS by 5.25 months from 16.75 to 22.00 months and 2-year survival rate by 12.5% from 29.2% to 41.7% (**B**) Representative images of ^{11}C-acetate PET, MRI, PET and MRI fusion in patients with IDH1-WT high-grade and IDH1-mt low-grade glioma. Red demarcation, ^{11}C-acetate PET-based tumor margin; Blue demarcation, MRI-based tumor margin. (**C**) The median SUVR on ^{11}C-acetate PET in IDH1-WT high-grade glioma (n=37) was significantly increased than that in low-grade or IDH1-mt glioma (n=58) (2.05 (Interquartile range (IQR) 1.77-2.41) versus 1.02 (IQR 0.92-1.30)) (**D**) The median tumor volume on ^{11}C-

acetate PET was significantly larger than that on MRI in IDH1-WT high-grade gliomas (n=37) (20.80 (IQR 8.99-59.39) versus 7.72 (IQR 1.80-26.14)) (**E-H**) Immunofluorescence images with GFAP, Ki-67, and MAO-B and immunohistochemistry images with MCT1 (brown) in human glioma tissues. Scale bars, 50 μm in e and f, and 20 μm in g and h. S, Star-shape astrocyte region; L, Linear-shape astrocyte region; T, Tumor region. (**I**) Immunofluorescence images with GFAP, Ki-67, and CD133 in IDH1-WT high-grade glioma tissues. (**J-M**) Quantification of GFAP, Ki-67, MAO-B, and MCT1 immunoreactivity in IDH1-WT high-grade versus IDH1-mt or low-grade gliomas (n=3). (**N**) The proportion of GFAP+ or CD133+ cells out of Ki-67+ cells in the S and L regions of IDH1-WT high-grade glioma tissues (n=4). Data are presented as median and IQR by Mann-Whitney U-test (**C, D**) and as mean ± SEM by unpaired two-tailed t-test (**J, L, K** right, **M, N**), or one-way ANOVA with Tukey (**K** left). **P < 0.01, ***P < 0.001, ****P < 0.0001.

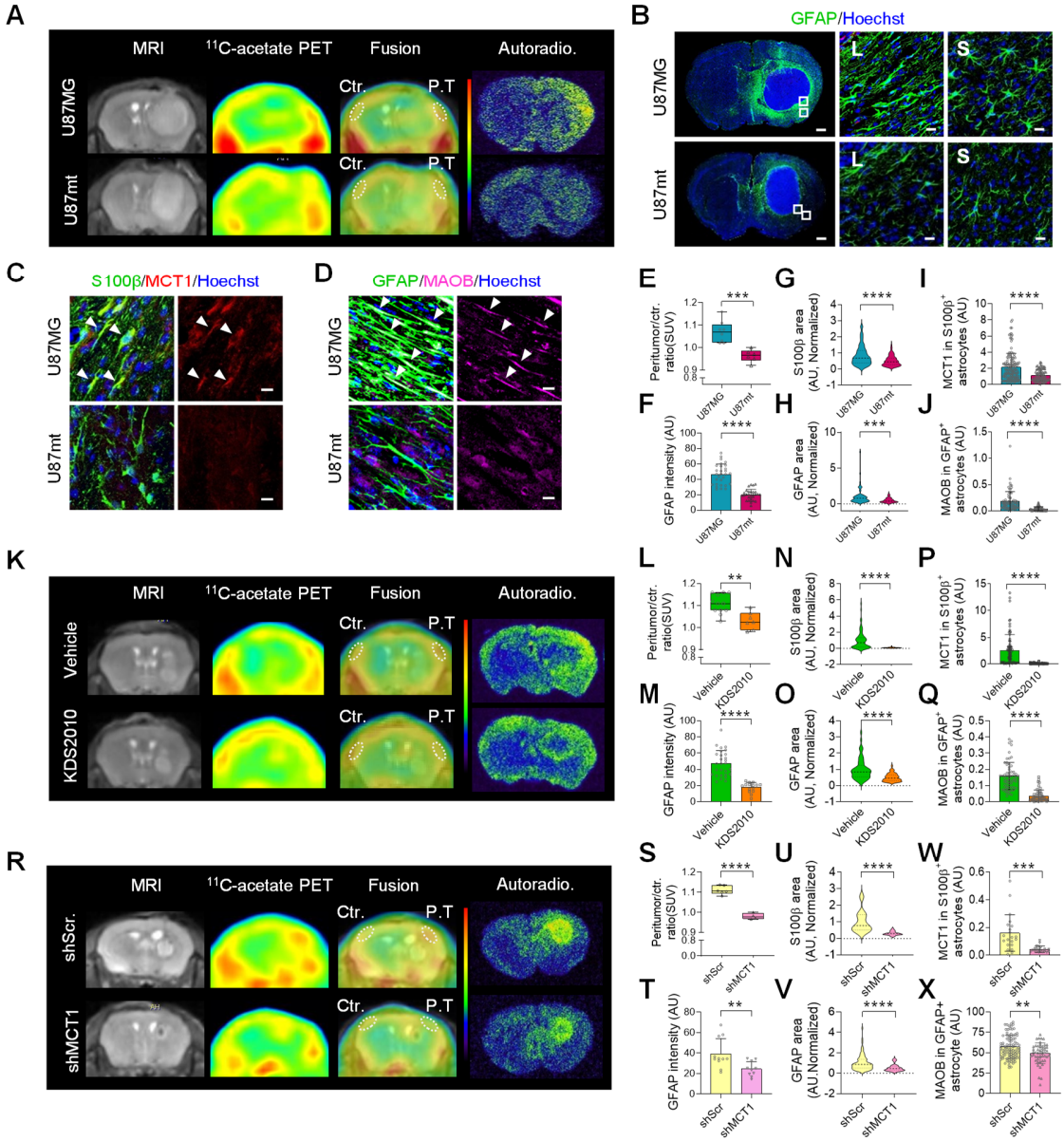

Figure 2. Control of reactive astrogliosis and acetate uptake by inhibition of MAO-B and MCT1 in mouse glioblastoma model. (**A**) Representative images of MRI, ^{11}C-acetate PET, PET and MRI fusion, and ^{14}C-acetate autoradiography in mouse glioma models of U87MG and U87mt**.** (**B**) Immunofluorescence images of GFAP expression in the mouse models. (**C-D**) Immunofluorescence images of S100β and MCT1 expressions, GFAP and MAO-B expressions in the mouse models. (**E**) SUVR of ^{11}C-acetate in the peri-tumoral and contralateral regions (*n*=5). (**F-J**) Quantification of GFAP, S100β, MCT1, and MAO-B expressions in the mouse models (*n*=3). (**K**) Representative images of MRI, ^{11}C-acetate PET, PET and MRI fusion, and ^{14}C-acetate autoradiography with or without KDS2010 administration in the U87MG mouse model. (**L**) SUVR of ^{11}C-acetate in the peri-tumoral and contralateral regions (*n*=5). (**M-Q**) Quantification of GFAP, S100β, MCT1, and MAO-B expressions with or without KDS2010 administration in U87MG mouse models (*n*=3). (**R**) Representative images of MRI, ^{11}C-acetate PET, PET and MRI fusion and ^{14}C-acetate autoradiography with or without astrocyte-specific MCT1 gene-silencing around U87MG cells. (**S**) SUVR of ^{11}C-acetate in the peri-tumoral and contralateral regions (*n*=5). (**T-X**) Quantification of GFAP, S100β, MCT1, and MAO-B expressions with or without

astrocyte-specific MCT1 gene-silencing of around U87MG cells (*n*=3). Data are presented as mean ± SEM. *P < 0.1, **P < 0.01, ***P < 0.001, ****P < 0.0001 by unpaired two-tailed t-test.

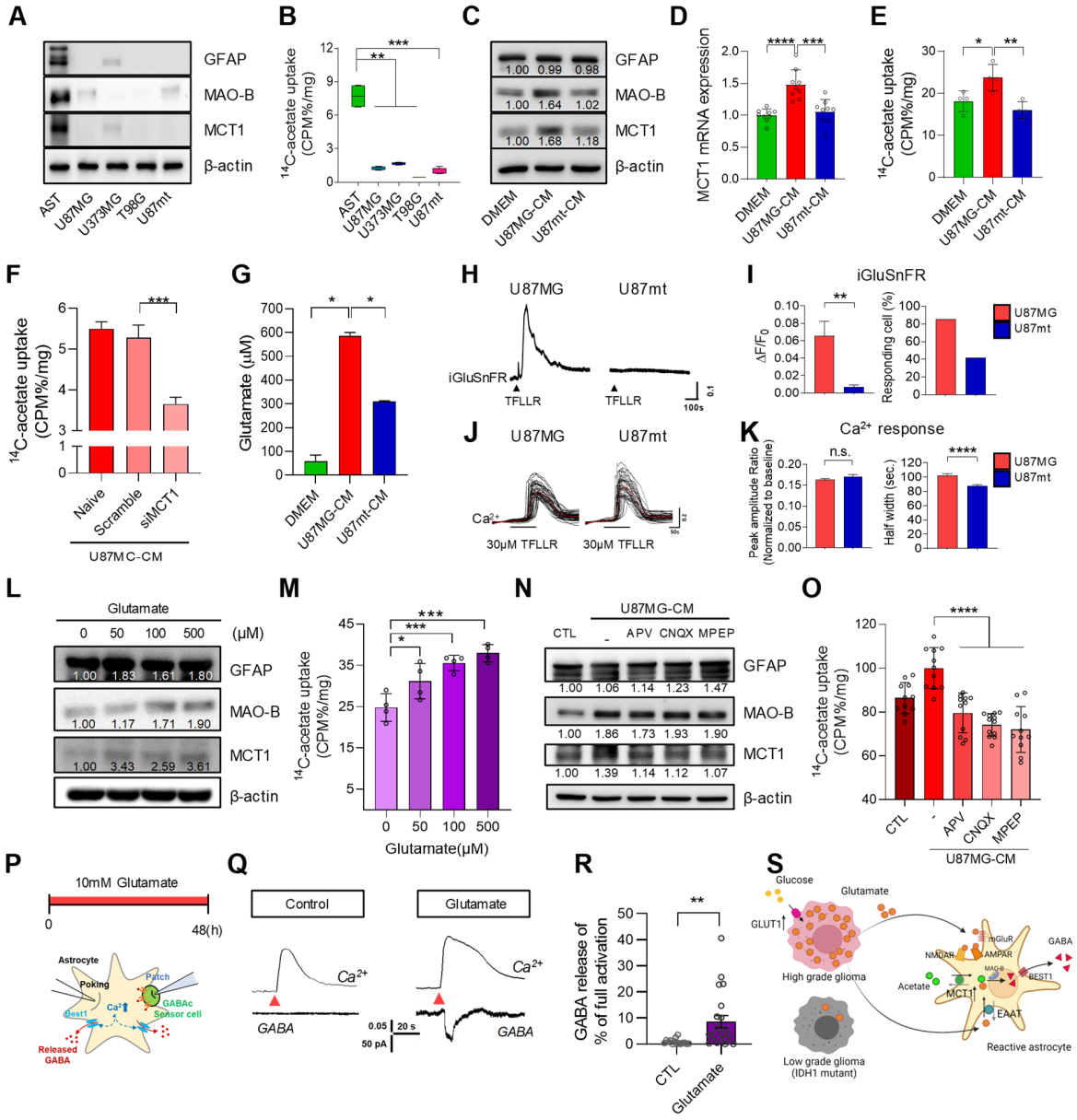

Figure 3. Excessive glutamate-release from high-grade glioma cells causes increased astrocytic ^{14}C-acetate uptake and aberrant GABA release. (**A-B**) Western-blot for GFAP, MAO-B, and MCT1 expressions and ^{14}C-acetate uptake in mouse primary astrocytes (AST) and various human GBM cell lines (U87MG, U373MG, T98G, and U87mt). (**C-E**) Western-blot for GFAP, MAO-B, and MCT1 expressions, MCT1 mRNA expressions, ^{14}C-acetate uptake of U87MG and U87mt-CM-treated astrocytes. (**F**) ^{14}C-acetated uptake after siMCT1- treatment in U87MG-CM-treated astrocytes. (**G**) Glutamate concentration in U87MG and U87mt-CM-treated astrocytes. (**H**) Representative traces of TFLLR-induced glutamate release from U87MG and U87mt cells recorded by iGluSnFR. (**I**) Quantification of TFLLR-induced iGluSnFR response ΔF/F0 and responding cell percentage. (**J**) Representative traces of TFLLR-induced Ca^{2+} response in U87MG and U87mt cells. (**K**) Quantification of TFLLR-induced Ca^{2+} peak amplitude ratio and half width. (**L-M**) Western blot analysis for GFAP, MAO-B and MCT1 expressions and ^{14}C-acetate uptake in astrocytes treated with L-glutamate. (**N-O**) Western blot images of GFAP, MAO-B, and MCT1 and ^{14}C-acetate uptake in astrocytes treated with U87MG-CM and APV, CNQX, or MPEP. (**P**) Schematic diagram of sniffer patch to record the astrocytic GABA release. (**Q**)

Representative traces of Ca^{2+} signal (top) and GABA current (bottom). Red arrowheads indicate the time-point of poking the astrocyte. (**R**) Quantification of poking-induced GABA current. (**S**) Schematic illustration summarizing a hypothesized mechanism. Data are presented as mean ± SEM. *P < 0.1, **P < 0.01, ***P < 0.001, n.s.: not significant by unpaired two-tailed t-test (**I, K, R**) or one-way ANOVA with Tukey.

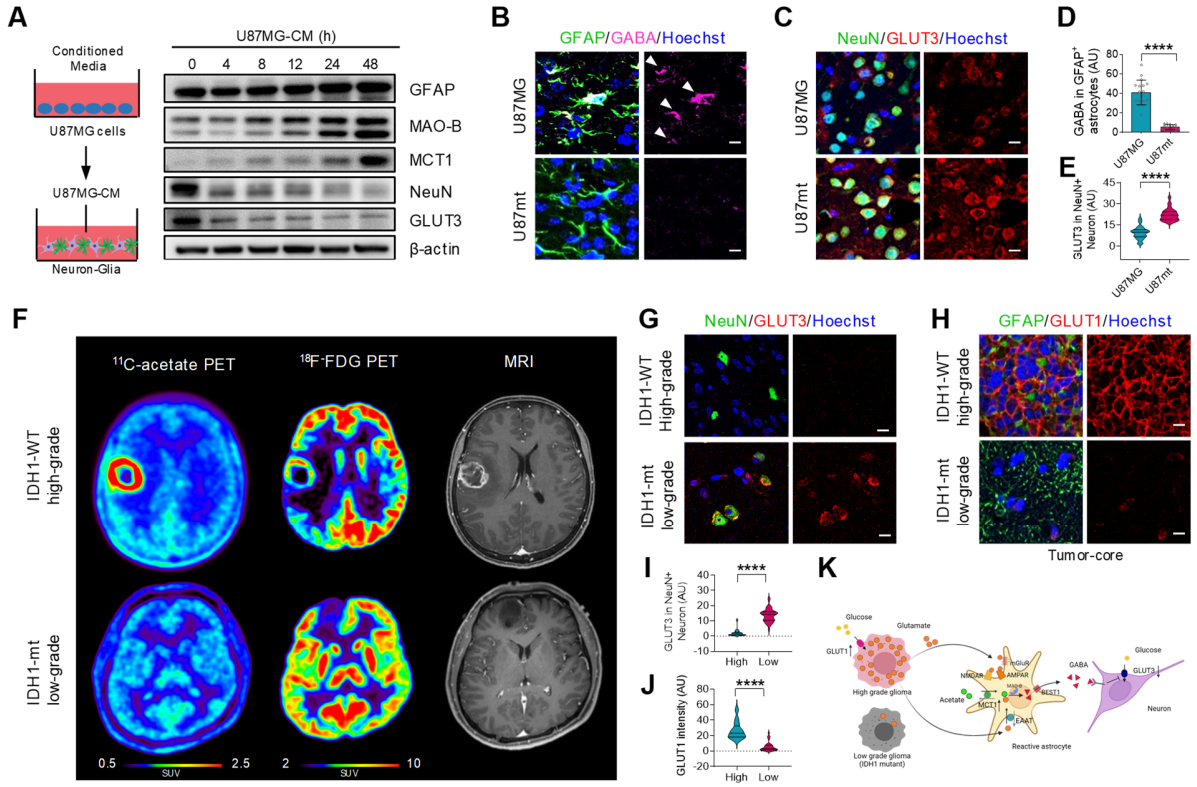

Figure 4. Astrocytic GABA suppresses neighbouring neuronal glucose uptake in neuron-glia co-culture, mouse U87MG model, and patient high-grade gliomas. (**A**) Schematic diagram (left) and western-blot analysis for GFAP, MAO-B, MCT1, NeuN, and GLUT3 from mouse primary neuron-glia co-culture treated with U87MG-CM. (**B, C**) Representative images of GFAP and GABA**,** NeuN and GLUT3 staining in U87MG and U87mt models. (**D, E**) Quantification of GABA and GLUT3 expression levels (*n*=3). (**F**) ^{11}C-acetate PET, ^{18}F-FDG PET, and MRI of patients with IDH1-WT high-grade glioma (top row) and IDH1-mt or low-grade glioma (bottom row). (**G, H**) Representative images of NeuN and GLUT3 in the peri-tumoral region (**G**) and GFAP and GLUT1 in the tumor core region (**H**) of glioma tissues from the patients. (**I, J**) Quantification of neuronal GLUT3 and tumoral GLUT1 expressions in human glioma tissues (*n*=3). (**K**) Schematic illustration summarizing a hypothesized mechanism. Data are presented as mean ± SEM., ***P < 0.001, ****P < 0.0001 by unpaired two-tailed t-test.